

**SUPPORTING INFORMATION**  
**for**

**Temperature-Dependent Transient Absorption Spectroscopy Elucidates Trapped-Hole Dynamics in CdS and CdSe Nanorods**

James K. Utterback, Jesse L. Ruzicka, Hayden Hamby, Joel D. Eaves, Gordana Dukovic\*

Department of Chemistry, University of Colorado Boulder, Boulder, Colorado 80309, USA

\*Correspondence to: [gordana.dukovic@colorado.edu](mailto:gordana.dukovic@colorado.edu)

**Table of Contents**

I.	Experimental .....	S2
II.	Transmission electron microscopy images .....	S3
III.	Temperature dependence of the TA bleach peak of CdS and CdSe nanorods .....	S4
IV.	Temperature dependence of charge separation in nonuniform CdS and CdSe nanorods..	S5
V.	Temperature dependence of electron relaxation in uniform CdS nanorods.....	S6
VI.	Upper and lower bounds for hole-hopping rate .....	S7
VII.	Absorption spectra of CdS and CdSe nanorods .....	S8
VIII.	References.....	S8

## I. Experimental

### *Synthesis and purification of CdS nanorods (NRs)*

Nonuniform CdS NRs were synthesized following established synthetic methods.<sup>1</sup> The CdS seeds were synthesized from a starting mixture containing 0.108 g cadmium oxide (CdO, 99.99% Aldrich), 0.604 g octadecylphosphonic acid (ODPA, 99%, PCI Synthesis), and 3.300 g trioctylphosphine oxide (TOPO, 99%, Aldrich). After heating to 320°C, a stock solution of the sulfur precursor (0.172 g hexamethyldisilathiane ((TMS)<sub>2</sub>S, synthesis grade, Aldrich) in 3 g of tributylphosphine (TBP, 97%, Aldrich)) was quickly injected. Nanocrystal growth proceeded for 3 min at 250°C. The reaction was stopped by removing the heating mantle and injecting 10 mL of a 1:1 (v/v) mixture of anhydrous methanol (99.8%, Sigma-Aldrich) and anhydrous toluene (99.8%, Sigma-Aldrich). The CdS seeds were then dissolved in a minimal amount of anhydrous toluene, precipitated with methanol to wash away unreacted precursor, and the final product was dissolved in trioctylphosphine (TOP, 97%, Strem). The purified CdS seeds had their lowest-energy exciton peak at 399 nm. The NRs were synthesized from a starting solution of 0.086 g CdO, 3 g TOPO, 0.292 g ODPA, and 0.084 g hexylphosphonic acid (HPA, 99%, PCI Synthesis). The solution was heated to 350°C followed by injection of 1.5 g of TOP. When the temperature of the Cd-containing solution stabilized at 350°C, the solution containing both CdS seeds and sulfur precursor—0.120 g of sulfur (S, 99.998%, Aldrich) in 1.5 g of TOP mixed with  $8 \times 10^{-8}$  mol CdS QD seeds—was quickly injected. Nanocrystal growth proceeded for 8 min, after which the solution was cooled and the particles were precipitated and purified with a 1:1:1 acetone/toluene/methanol mixture. After purification, the NRs were size-selected through a precipitation process by slowly increasing the polarity of a nanocrystal-toluene solution with isopropanol.

### *Synthesis and purification of CdSe NRs*

The synthesis for nonuniform CdSe NRs was adapted from a previously reported procedure.<sup>2</sup> The synthesis of the batch of CdSe NRs used in the experiments presented here was described in detail previously.<sup>3</sup>

### *Ligand exchange*

The hydrophobic native surface-capping ligands of both the as-synthesized CdS and CdSe NRs were replaced with 3-mercaptoproponate (3-MPA) ligands following a previously reported procedure,<sup>4</sup> and the resulting particles were redispersed in anhydrous methanol.

### *UV-visible absorption spectroscopy*

The samples used for UV-visible absorption contained CdS NRs or CdSe NRs capped with 3-MPA ligands, dispersed in 4:1 ethanol:methanol (v/v), and were sealed under Ar in a 1 cm × 1 cm quartz cuvette. UV-visible absorption spectra were recorded using an Agilent 8453 spectrophotometer equipped with tungsten and deuterium lamps.

### *Transmission electron microscopy*

Transmission electron micrograph (TEM) samples were prepared by drop-casting CdS and CdSe NRs with native ligands onto TEM grids (300 mesh copper grids with carbon film, Electron Microscopy Science). TEM images in Figure S1 were collected on a FEI Tecnai Spirit BioTwin operating at 120 kV. The dimensions of the NRs were determined by measuring more than 200 particles in TEM using ImageJ software.<sup>5</sup> High-resolution TEM images (Figure 1) were collected on a FEI Tecnai ST20 operating at 200 kV.

### *Transient absorption (TA) spectroscopy*

The complete experimental set-up used for TA experiments here has been described previously.<sup>6</sup> Briefly, femtosecond TA spectroscopy measurements in the 100 fs–to–3 ns time window were performed using a regeneratively amplified Ti:sapphire laser (Solstice, Spectra-Physics, 800 nm, 100 fs, 1 kHz, 3.5 mJ/pulse), an optical parametric amplifier (TOPAS-C, Light Conversion), and a HELIOS spectrometer (Ultrafast Systems, LLC) with the white-light continuum being generated from the 800 nm Solstice output using a sapphire plate. Nanosecond TA spectroscopy (0.3 ns to 400  $\mu$ s) was performed using an EOS spectrometer (Ultrafast Systems, LLC) where the white-light probe beam (400–900 nm, 0.3 ns, 2 kHz) was generated by a Nd:YAG laser focused into a photonic crystal fiber and the pump-probe delay was controlled by an electronic delay generator (CNT-90, Pendulum Instruments). The pump and probe beams were focused and overlapped on the sample, and the probe beam was split into probe and reference detection channels.

Temperature dependence studies were carried out using a Janis STVP-100 continuous flow optical cryostat with quartz windows equipped with a home-built 1 cm cuvette holder. The samples were held in a 1 cm cryogenic cuvette from FireflySci (type 66FL) equipped with a screw cap. The cuvette was cooled under flowing nitrogen vapor and the temperature was controlled with a LakeShore 335 temperature controller connected to two thermocouple/heating element pairs, one at the head of the sample holder and the other in the vaporizer assembly located at the bottom of the cryostat.

## II. Transmission electron microscopy images

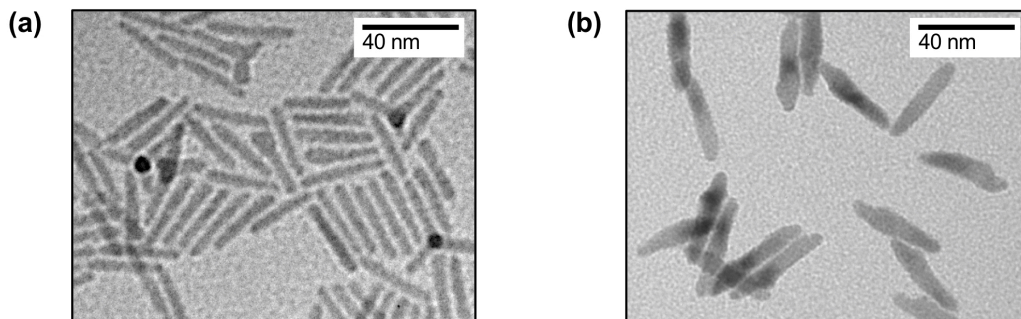


**Figure S1.** Transmission electron microscopy images of (a) CdS and (b) CdSe NRs. In the samples of NRs studied here, many NRs are nonuniform in diameter.

### III. Temperature dependence of the TA bleach peak of CdS and CdSe nanorods

Figure S2 shows the centers and widths of the main bleach peak of CdS and CdSe NRs from Figure 2 as a function of temperature. The peak shifting in Figure S2a was fit to a line, giving  $-\partial E_{\max}/\partial T$  values of  $(3.6 \pm 0.2) \times 10^{-4}$  eV/K and  $(2.4 \pm 0.2) \times 10^{-4}$  eV/K for CdS and CdSe NRs, respectively. These values are consistent with previous reports for bulk and nanocrystalline CdS and CdSe.<sup>7</sup> The width of the main bleach feature in Figure S2b, measured as the full width at half maximum (FWHM), was fit to a previously described model:<sup>8</sup>  $\Gamma(T) = \Gamma_{\text{inh}} + \sigma T + \Gamma_{\text{LO}}(e^{-E_{\text{LO}}/k_{\text{B}}T} - 1)^{-1}$ , where  $\Gamma(T)$  is the temperature-dependent linewidth,  $\Gamma_{\text{inh}}$  is the temperature-independent inhomogeneous linewidth,  $\sigma$  is the exciton–acoustic phonon coupling coefficient,  $\Gamma_{\text{LO}}$  is the band-edge exciton–LO phonon coupling coefficient,  $E_{\text{LO}}$  is the LO phonon energy,  $k_{\text{B}}$  is the Boltzmann constant, and  $T$  is the temperature. Fits were performed using known values of  $\sigma = 0.2$   $\mu\text{eV/K}$  and  $E_{\text{LO}} = 36.8$  meV for CdS NRs,<sup>8-10</sup> and  $\sigma = 8$   $\mu\text{eV/K}$  and  $E_{\text{LO}} = 26.1$  meV for CdSe NRs,<sup>8,11-13</sup> giving  $\Gamma_{\text{inh}} = 28 \pm 1$  meV and  $\Gamma_{\text{LO}} = 51 \pm 2$  meV for CdS NRs, and  $\Gamma_{\text{inh}} = 58 \pm 4$  and  $\Gamma_{\text{LO}} = 65 \pm 9$  meV for CdSe NRs. These values of  $\Gamma_{\text{inh}}$  are consistent with the polydispersity of each sample and the values of  $\Gamma_{\text{LO}}$  are consistent with previous reports for bulk and nanocrystalline CdS and CdSe.<sup>8</sup> This analysis shows that the changes in the peak centers and widths of the main TA bleach peak with temperature are quantitatively consistent with expected trends for CdS and CdSe nanocrystals. This spectral shifting with temperature was accounted for when spectral averaging was performed in order to isolate rod and bulb decay traces (see Methods).

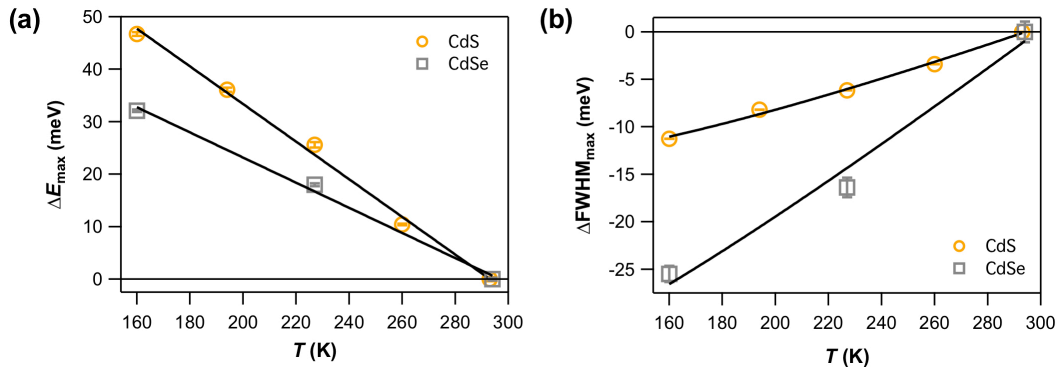


**Figure S2.** Characterization of the main TA bleach peak as a function of temperature for CdS and CdSe NRs, measured 100–300 ns and 1–3 ns after excitation, respectively. (a) Bleach peak shift,  $\Delta E_{\max}$ , relative to 294 K. At 294 K,  $E_{\max}$  is 2.7112 and 1.8848 eV for CdS and CdSe NRs, respectively. (b) Bleach peak width,  $\Delta \text{FWHM}_{\max}$ , relative to 294 K. At 294 K,  $\text{FWHM}_{\max}$  is 43 and 97 meV for CdS and CdSe NRs, respectively.

#### IV. Temperature dependence of charge separation in nonuniform CdS and CdSe nanorods

Figure S3 demonstrates rod-to-bulb electron population transfer in nonuniform CdS and CdSe NRs. In all experiments presented here, the CdS and CdSe NRs were excited above the band gap, which primarily excite the rods rather than the bulbs because they comprise a larger volume fraction of the nanostructures.<sup>3,14-17</sup> Driven by the lower confinement energy of the bulb state compared to the rod state in nonuniform NRs, photoexcited electrons that are initially generated in the rod morphological feature transfer to the bulb. As has been demonstrated before in room temperature TA studies,<sup>3,15,17,18</sup> this process manifests as a partial decay of the rod signal (Figure S3a,b) and a corresponding rise of the bulb signal (Figure S3c,d). Here we find that, in CdS NRs, the TA time traces overlap within the noise at each temperature studied, indicating that the kinetics of rod-to-bulb electron localization do not depend strongly on temperature over the 160–294 K range. At all temperatures, rod-to-bulb electron localization constitutes  $\sim 25\%$  of the decay and is complete after a few hundred picoseconds in CdS NRs. In CdSe NRs the extent of electron localization depends on the temperature, reaching 68%, 73% and 100% at 294, 227 and 160 K, respectively. Localization is complete after a few hundred picoseconds at each temperature. Hole trapping in CdS and CdSe nanocrystals is fast in comparison, occurring on a sub-picosecond timescale.<sup>3,19-28</sup> These observations suggest that spatial separation between the electron localized in the bulb and the hole trapped on the rod occurs at each temperature studied.

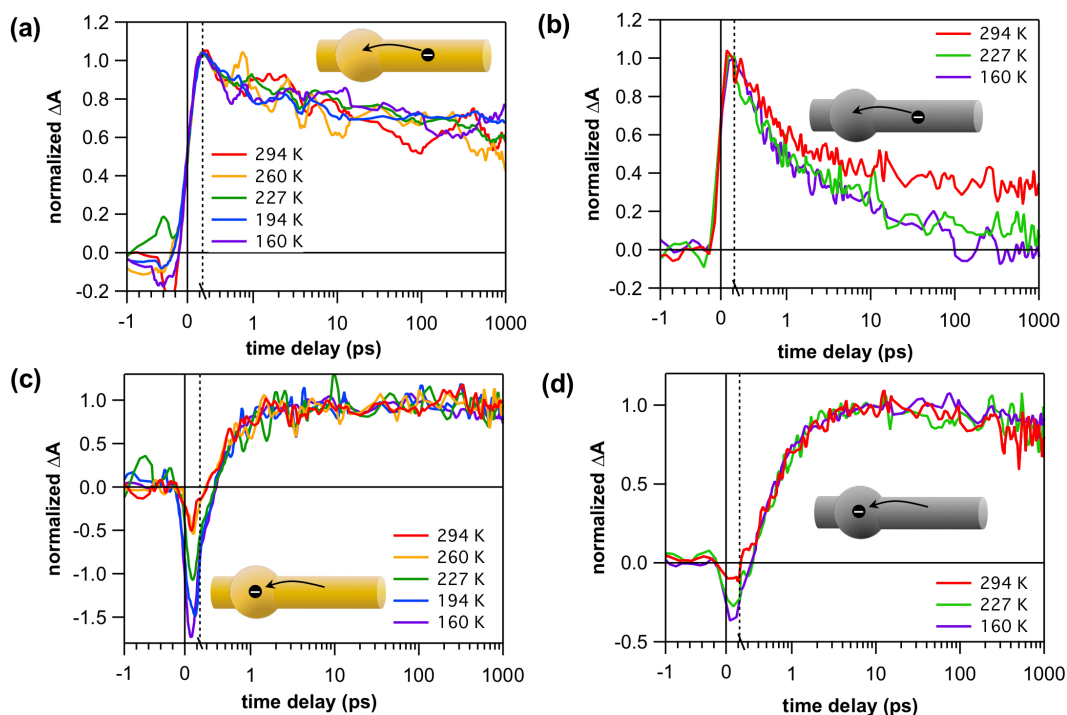


**Figure S3.** Rod-to-bulb electron localization in CdS and CdSe NRs for temperatures in the range of 160 to 294 K. Formation and partial decay of rod signal in (a) CdS NRs after 400 nm excitation and (b) CdSe NRs after 600 nm excitation, and corresponding rise of bulb signal in (c) CdS NRs and (d) CdSe NRs, collected at indicated temperatures. Time traces for isolated rod and bulb signals were obtained by averaging traces at the wavelengths reported in the Methods section of the manuscript. All traces are normalized to have maximum amplitudes of 1. The time axes are linear for the first 0.25 ps and logarithmic thereafter.

## V. Temperature dependence of electron relaxation in uniform CdS nanorods

The rod signal remaining after electron localization is complete is due to uniform NRs in the sample.<sup>3,17</sup> The TA decay traces that correspond to electron dynamics in uniform CdS NRs after the timescale of rod-to-bulb electron localization at different temperatures are shown below. These decay traces are due to uniform NRs in solution. In contrast to the power-law recombination dynamics of spatially separated electrons and trapped holes in nonuniform NRs (Figure 2), spatially overlapping electrons and trapped holes in uniform NRs exhibit exponential asymptotic decay at all temperatures. The timescale of the exponential tail, which is likely due to recombination, increases as temperature decreases. Additionally, as the temperature is reduced, a broad, non-exponential, pre-asymptotic decay component emerges that precedes the exponential cutoff, similar to the pre-asymptotic decay of nonuniform NRs (Figure 2 and S5). The existence of this behavior in both uniform and nonuniform NRs suggests a common mechanism that is unrelated to trapped-hole diffusion, such as electron trapping with a distribution in trapping rates. Nonetheless, the asymptotic exponential tail in uniform NRs and the power-law tail in nonuniform NRs are easily distinguished from this pre-asymptotic decay component.

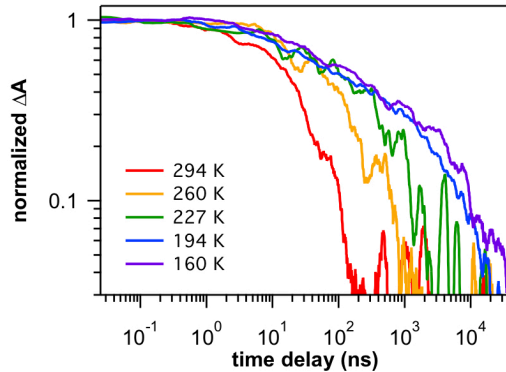


**Figure S4.** TA time traces of rod signal in uniform CdS NRs over 160–294 K. Time traces for the isolated rod signals at each temperature were obtained by averaging traces at the wavelengths reported in the Methods section of the manuscript.

We do not have data analogous to Figure S4 for CdSe NRs because the extent of electron localization is high (Figure S3b) and there are few uniform NRs in the sample.

## VI. Upper and lower bounds for hole-hopping rate

Here we describe how we obtained upper and lower bounds for the hole-hopping rate presented in the manuscript. The pre-asymptotic decay of the charge-separated state in Figure 2 depends on temperature. As the temperature decreases, the entrance into the power-law occurs at progressively longer times. For times after rod-to-bulb electron localization we assume a form for the bulb electron survival probability,  $S(t)$ , that comes from one-dimensional diffusion–annihilation where all trapped holes start at the same distance from the bulb,  $z_0$ , and diffuse with diffusion coefficient  $D$ . This is a reasonable approximation because for long times  $S(t)$  will be insensitive to the shape of the distribution of the initial positions and depends only on the mean,  $z_0$ .<sup>17</sup> In this regime,

$$S(t) = \text{erf}\left(\sqrt{\tau/t}\right), \quad (\text{S1})$$

where the  $\tau = z_0^2/4D$ .<sup>17,29</sup> Expanding  $S(t)$  asymptotically for long times yields the power law:  $S(t) \propto t^{-1/2}$ . Because the onset of the power-law tail occurs for all times  $t > \tau$  in eq S1, we take the upper bound for  $\tau$  to be the time at which the power-law tail begins (Figure S5a), defined as the time at which relative difference between a fit to a  $t^{-1/2}$  power-law tail and the data reached 5%. Separately, we obtained the lower bound for  $\tau$  by matching eq S1 to the initial decay as well as the power-law tail (Figure S5a). This gives the smallest possible value for  $\tau$  because any smaller value would underestimate the amplitude of the signal at late times;  $\tau$  cannot be any smaller because additional decay components would act to reduce the amplitude at late times even further. These definitions for the upper and lower bounds of  $\tau$  are illustrated using CdS NRs at 260 K as an example in Figure S5a, and the fits to every CdS and CdSe NR trace are shown in Figures S5b,c.

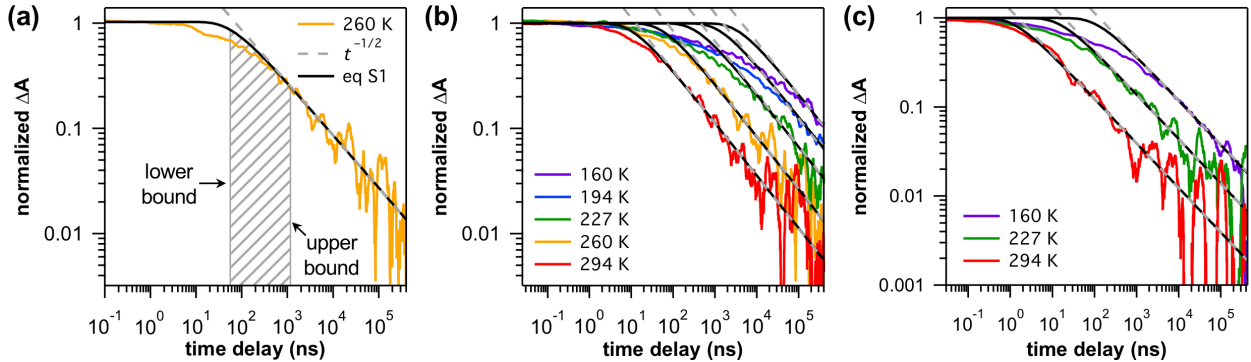


**Figure S5.** Obtaining upper and lower bounds of  $\tau$  for CdS and CdSe NRs as a function of temperature. (a) Illustrative example of obtaining upper and lower bounds of  $\tau$  for CdS NRs at 260 K. The upper bound is the onset of the power-law tail while the lower bound is found by fitting the beginning and tail of the decay trace to eq S1. The shaded region represents the range of possible  $\tau$  values. (b) Fits of eq S1 and the power-law tail for CdS NRs at the indicated temperatures. (c) Fits of eq S1 and the power-law tail for CdSe NRs at the indicated temperatures.

## VII. Absorption spectra of CdS and CdSe nanorods

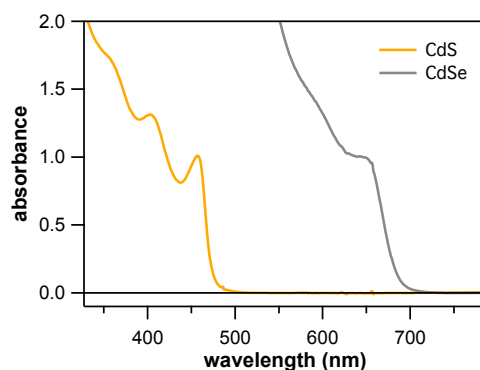


**Figure S6.** Room-temperature UV-visible absorption spectra of CdS and CdSe NRs in 4:1 ethanol:methanol (v/v).

## VIII. References

1. Carbone, L.; Nobile, C.; De Giorgi, M.; Sala, F. D.; Morello, G.; Pompa, P.; Hytch, M.; Snoeck, E.; Fiore, A.; Franchini, I. R., et al., Synthesis and micrometer-scale assembly of colloidal CdSe/CdS nanorods prepared by a seeded growth approach. *Nano Lett.*, **2007**, *7*, 2942-2950.
2. Lee, D.; Kim, W. D.; Lee, S.; Bae, W. K.; Lee, S.; Lee, D. C., Direct Cd-to-Pb exchange of CdSe nanorods into PbSe/CdSe axial heterojunction nanorods. *Chem. Mater.*, **2015**, *27*, 5295-5304.
3. Utterback, J. K.; Hamby, H.; Pearce, O.; Eaves, J. D.; Dukovic, G., Trapped-hole diffusion in photoexcited CdSe nanorods. *J. Phys. Chem. C*, **2018**, *122*, 16974-16982.
4. Brown, K. A.; Wilker, M. B.; Boehm, M.; Dukovic, G.; King, P. W., Characterization of photochemical processes for H<sub>2</sub> production by CdS nanorod-[FeFe] hydrogenase complexes. *J. Am. Chem. Soc.*, **2012**, *134*, 5627-5636.
5. Schneider, C. A.; Rasband, W. S.; Eliceiri, K. W., NIH Image to ImageJ: 25 years of image analysis. *Nat. Methods*, **2012**, *9*, 671-675.
6. Tseng, H. W.; Wilker, M. B.; Damrauer, N. H.; Dukovic, G., Charge transfer dynamics between photoexcited CdS nanorods and mononuclear Ru water-oxidation catalysts. *J. Am. Chem. Soc.*, **2013**, *135*, 3383-3386.
7. Madelung, O., *Semiconductors—Basic Data*. 2nd ed.; Springer: Berlin, 1996.
8. Rudin, S.; Reinecke, T. L.; Segall, B., Temperature-dependent exciton linewidths in semiconductors. *Phys. Rev. B*, **1990**, *42*, 11218-11231.
9. Shiang, J. J.; Risbud, S. H.; Alivisatos, A. P., Resonance Raman studies of the ground and lowest electronic excited-state in CdS nanocrystals. *J. Chem. Phys.*, **1993**, *98*, 8432-8442.
10. Kulik, D.; Htoon, H.; Shih, C. K.; Li, Y. D., Photoluminescence properties of single CdS nanorods. *J. Appl. Phys.*, **2004**, *95*, 1056-1063.
11. Gindele, F.; Hild, K.; Langbein, W.; Woggon, U., Temperature-dependent line widths of single excitons and biexcitons. *J. Lumin.*, **2000**, *87-9*, 381-383.
12. Lange, H.; Artemyev, M.; Woggon, U.; Thomsen, C., Geometry dependence of the phonon modes in CdSe nanorods. *Nanotechnology*, **2009**, *20*, 045705.
13. Beecher, A. N.; Dziatko, R. A.; Steigerwald, M. L.; Owen, J. S.; Crowther, A. C., Transition from molecular vibrations to phonons in atomically precise cadmium selenide quantum dots. *J. Am. Chem. Soc.*, **2016**, *138*, 16754-16763.

14. Yu, W. W.; Qu, L.; Guo, W.; Peng, X., Experimental determination of the extinction coefficient of CdTe, CdSe, and CdS nanocrystals. *Chem. Mater.*, **2003**, *15*, 2854-2860.
15. Wu, K. F.; Rodriguez-Cordoba, W. E.; Liu, Z.; Zhu, H. M.; Lian, T. Q., Beyond band alignment: Hole localization driven formation of three spatially separated long-lived exciton states in CdSe/CdS nanorods. *ACS Nano*, **2013**, *7*, 7173-7185.
16. Yang, Y.; Wu, K. F.; Chen, Z. Y.; Jeong, B. S.; Lian, T. Q., Competition of branch-to-core exciton localization and interfacial electron transfer in CdSe tetrapods. *Chem. Phys.*, **2016**, *471*, 32-38.
17. Utterback, J. K.; Grennell, A. N.; Wilker, M. B.; Pearce, O.; Eaves, J. D.; Dukovic, G., Observation of trapped-hole diffusion on the surfaces of CdS nanorods. *Nat. Chem.*, **2016**, *8*, 1061-1066.
18. Wu, K.; Rodriguez-Cordoba, W.; Lian, T., Exciton localization and dissociation dynamics in CdS and CdS-Pt quantum confined nanorods: Effect of nonuniform rod diameters. *J. Phys. Chem. B*, **2014**, *118*, 14062-14069.
19. Klimov, V.; Bolivar, P. H.; Kurz, H., Ultrafast carrier dynamics in semiconductor quantum dots. *Phys. Rev. B*, **1996**, *53*, 1463-1467.
20. Klimov, V. I.; Schwarz, C. J.; McBranch, D. W.; Leatherdale, C. A.; Bawendi, M. G., Ultrafast dynamics of inter- and intraband transitions in semiconductor nanocrystals: Implications for quantum-dot lasers. *Phys. Rev. B*, **1999**, *60*, R2177-R2180.
21. Underwood, D. F.; Kippeny, T.; Rosenthal, S. J., Ultrafast carrier dynamics in CdSe nanocrystals determined by femtosecond fluorescence upconversion spectroscopy. *J. Phys. Chem. B*, **2001**, *105*, 436-443.
22. Burda, C.; Link, S.; Mohamed, M.; El-Sayed, M., The relaxation pathways of CdSe nanoparticles monitored with femtosecond time-resolution from the visible to the IR: Assignment of the transient features by carrier quenching. *J. Phys. Chem. B*, **2001**, *105*, 12286-12292.
23. McArthur, E. A.; Morris-Cohen, A. J.; Knowles, K. E.; Weiss, E. A., Charge carrier resolved relaxation of the first excitonic state in CdSe quantum dots probed with near-infrared transient absorption spectroscopy. *J. Phys. Chem. B*, **2010**, *114*, 14514-14520.
24. Knowles, K. E.; McArthur, E. A.; Weiss, E. A., A multi-timescale map of radiative and nonradiative decay pathways for excitons in CdSe quantum dots. *ACS Nano*, **2011**, *5*, 2026-2035.
25. Wu, K. F.; Zhu, H. M.; Liu, Z.; Rodriguez-Cordoba, W.; Lian, T. Q., Ultrafast charge separation and long-lived charge separated state in photocatalytic CdS-Pt nanorod heterostructures. *J. Am. Chem. Soc.*, **2012**, *134*, 10337-10340.
26. Keene, J. D.; McBride, J. R.; Orfield, N. J.; Rosenthal, S. J., Elimination of hole-surface overlap in graded CdS<sub>x</sub>Se<sub>1-x</sub> nanocrystals revealed by ultrafast fluorescence upconversion spectroscopy. *ACS Nano*, **2014**, *8*, 10665-10673.
27. Li, X.; Feng, D. H.; Tong, H. F.; Jia, T. Q.; Deng, L.; Sun, Z. R.; Xu, Z. Z., Hole surface trapping dynamics directly monitored by electron spin manipulation in CdS nanocrystals. *J. Phys. Chem. Lett.*, **2014**, *5*, 4310-4316.
28. Utterback, J. K.; Wilker, M. B.; Mulder, D. W.; King, P. W.; Eaves, J. D.; Dukovic, G., Quantum efficiency of charge transfer competing against nonexponential processes: The case of electron transfer from CdS nanorods to hydrogenase. *J. Phys. Chem. C*, **2019**, *123*, 886-896.
29. Redner, S., *A guide to first-passage processes*. Cambridge University Press: Cambridge, **2001**.